Peroxisome proliferator-activated receptor α regulates acesulfame-K-induced NAFLD via hepatic PLCβ: Foe and friend

PENG-YAO LIN[1*], JIA-RONG XIE[1*], TIAN-CHEN QIAN[2], SHI-SONG WANG[1], SI-YI YU[1], WEN-BO SHI[3], YING WANG[3], LU-ZE CEN[3], QING-JING ZHU[2], YI-YANG ZHENG[1], HUI GAO[1], RONG FANG[4], ZHAO-XIA XIA[4], AI-MING LIU[3] and LEI XU[1]

[1]Department of Gastroenterology, The First Affiliated Hospital of Ningbo University, Ningbo, Zhejiang 315010, P.R. China; [2]Department of Gastroenterology, The First Affiliated Hospital, College of Medicine, Zhejiang University, Hangzhou, Zhejiang 310027, P.R. China; [3]Department of Pharmacology, Health Science Center, Ningbo University, Ningbo, Zhejiang 315211, P.R. China; [4]Ningbo Clinical Pathology Diagnosis Center, Ningbo, Zhejiang 315021, P.R. China

Received October 30, 2025; Accepted January 28, 2026

DOI: 10.3892/ijmm.2026.5773

Abstract. Food additive acesulfame-K (AK), a non-nutritive sweetener, is widely used as a low-calorie sugar substitute to reduce energy intake. However, its potential impact on nonalcoholic fatty liver disease (NAFLD) and the involvement of peroxisome proliferator-activated receptor α (PPARα) remain unclear. In the present study, male wild-type (WT) and PPARα-null (KO) mice fed a 60% high-fat diet were treated with AK (2 mg/ml) in drinking water for 12 weeks to evaluate the effects of chronic AK exposure on NAFLD progression and the role of PPARα. PPARα inhibition and activation strategies were further applied in *in vivo* and *in vitro* models to validate the key findings. AK supplementation markedly increased hepatic lipid accumulation and impaired glucose tolerance through activation of phospholipase C beta (PLCβ) in hepatic sweet taste receptor (STR) signaling in the WT mice, but not in the KO mice. Consistently, PLCβ activation was observed in AK-induced lipid accumulation in Hepa1-6 and Huh-7 cells and was abolished by PPARα knockdown or inhibition. Pharmacological activation of PPARα mitigated AK-induced NAFLD progression by suppressing PLCβ activation in STR signaling. These findings demonstrated that chronic AK intake exacerbates NAFLD progression via PLCβ activation in hepatic STR signaling and that PLCβ activation depends on physiological PPARα activity. Pharmacological PPARα activation exerts a protective effect, highlighting the dual roles of PPARα in regulating AK-associated NAFLD risk.

Correspondence to: Dr Lei Xu, Department of Gastroenterology, The First Affiliated Hospital of Ningbo University, 59 Liuting Street, Ningbo, Zhejiang 315010, P.R. China
E-mail: xulei22@163.com

Dr Ai-Ming Liu, Department of Pharmacology, Health Science Center, Ningbo University, 818 Fenghua Road, Ningbo, Zhejiang 315211, P.R. China
E-mail: liuaiming@nbu.edu.cn

[*]Contributed equally

Abbreviations: ADI, acceptable daily intake; AK, acesulfame-K; ALT, alanine aminotransferase; AST, aspartate aminotransferase; AUC, area under the curve; DGKH, diacylglycerol kinase eta; DAG, diacylglycerol; FFA, free fatty acid; GNAT3, G protein subunit alpha transducin 3; HFD, high-fat diet; ITT, insulin tolerance test; KO, PPARα-null; NAFLD, nonalcoholic fatty liver disease; NASH, nonalcoholic steatohepatitis; NNS, non-nutritive sweetener; OGTT, oral glucose tolerance test; PKC, protein kinase C; PLCβ, phospholipase C beta; PPARα, peroxisome proliferator-activated receptor α; RNA-seq, RNA sequencing; RT-qPCR, reverse transcription-quantitative PCR; STR, sweet taste receptor; TAS1R2, taste 1 receptor member 2; TAS1R3, taste 1 receptor member 3; TC, total cholesterol; TG, triglycerides; WT, wild-type

Key words: peroxisome proliferator-activated receptor α, acesulfame-K, nonalcoholic fatty liver disease, phospholipase C beta, sweet taste receptor

Introduction

Nonalcoholic fatty liver disease (NAFLD) is a spectrum of liver diseases, initially characterized by the hepatic fat accumulation in those who consume little or no alcohol (1). Progressive histological features include simple steatosis, nonalcoholic steatohepatitis (NASH), cirrhosis, and hepatocellular carcinogenic transformation (2). NAFLD is becoming increasingly epidemic, affecting 25-40% of the global population (3). NAFLD is notably associated with metabolic disorders such as obesity and metabolic syndrome (3). The consumption of free sugar in liquid form is becoming popular, causing an elevated risk of NAFLD (4,5). Free sugar stimulates food intake by modulating appetite-regulating neural circuits and hormones, providing a key carbon source for *de novo* lipogenesis in the liver (5,6). Disordered glucose metabolism drives hepatic lipid accumulation and inflammatory responses, leading to NAFLD progression to NASH, cirrhosis, and hepatocellular carcinoma (2).

Non-nutritive sweeteners (NNSs), known as artificial sweeteners or noncaloric sweeteners, are food additives

that can modify the flavor of food and beverages without contributing considerable calories or nutrients (7). NNSs have been increasingly incorporated into diverse applications across the food industry, pharmaceutical formulations, and consumer goods sectors (8). The United States Food and Drug Administration has approved aspartame, sucralose, acesulfame-K (AK), saccharin, neotame and advantame as NNSs (9). The global NNS market ($91.2billion in 2023) is projected to grow at a compound annual growth rate of 2.51%, reaching $116.8 billion by 2033 (10). For each compound, the acceptable daily intake (ADI) was established based on the results from toxicological studies to ensure public safety (7,11). However, emerging evidence indicates that these compounds are involved in metabolic dysregulation (11,12). Prolonged exposure to NNSs is associated with an increased risk of cardiovascular events (13,14). Moreover, exposure to high doses of NNSs disrupts T-cell proliferation and differentiation (15). Nevertheless, to the best of the authors' knowledge, the mechanism by which chronic AK consumption affects the hepatic lipid metabolism is currently unexplored.

Sweet taste receptors (STRs) are the representative class C members of the G protein-coupled receptor family (16). Different taste signals are mediated by distinct receptor combinations (16). Taste 1 receptor member 2 and 3 (TAS1R2 and TAS1R3) form a heterodimer that serves as an STR on taste bud cells to perceive sweet substances (16,17). Natural monosaccharides, disaccharides, and synthetic sweeteners can serve as ligands that activate the sweet receptor protein (18). Importantly, STRs are not limited to the oral cavity but are also expressed in several other tissues, including the liver (19). STRs in the small intestine facilitate glucose absorption and the secretion of gut endocrine hormones (20). In sweet taste signal transduction, Phospholipase C beta (PLCβ) serves as a key effector that catalyzes the hydrolysis of membrane phosphatidylinositol 4,5-bisphosphate (21). This reaction generates the second messengers, inositol trisphosphate and diacylglycerol (DAG), triggering Ca^{2+} release from intracellular stores and protein kinase C (PKC) activation (21). However, research on the presence and activity of STRs in the liver remains to be conducted. AK exhibits remarkable metabolic stability compared with other NNSs. It is absorbed as native form from the small intestine through the portal vein to activate STRs in the liver (8). It is unclear how the metabolic alterations resulting from STR activation in the liver are regulated.

Peroxisome proliferator-activated receptor α (PPARα) is highly expressed in the liver, where it regulates genes involved in glucolipid metabolism (22,23). Elevated free fatty acids during fasting activate PPARα, enhancing hepatic β-oxidation to reduce lipid accumulation and lipotoxicity. Thus, PPARα improves insulin sensitivity and glucose homeostasis by suppressing gluconeogenesis (24). PPARα activation also increases fibroblast growth factor 21 production, enhancing glucose uptake and insulin sensitivity to regulate glucose metabolism (25). High glucose and free fatty acid levels lead to the accumulation of lipid intermediates and the subsequent activation of PKC (26). While PPARα serves as a key modulator of glucose metabolism, its regulatory effect on the metabolic action of NNSs remains unknown.

In the present study, AK was administered in drinking water to mice on a high-fat diet (HFD) to assess its effects on NAFLD progression, with a focus on the role of PPARα. *In vivo* and *in vitro* models were used to substantiate the targets of STR signaling pathways regulated by PPARα.

Materials and methods

Materials and reagents. An HFD (cat. no. D12492) and standard chow diet (cat. no. XTI01SL-002) were procured from Research Diets, Inc. and Jiangsu Xietong Pharmaceutical Bio-Engineering Co., Ltd., respectively. Detailed nutritional composition of the diets is provided in Data S1. Serum lipid profiles, including total cholesterol (TC; cat. no. H202) and triglycerides (TG; cat. no. H201), were analyzed using commercial assay kits from Ningbo Meikang Biotechnology Co., Ltd. Hepatic function biomarkers, alanine aminotransferase (ALT) and aspartate aminotransferase (AST), were quantified with kits from the same supplier. Fetal bovine serum was obtained from PAN-Seratech GmbH. Ready-to-use penicillin-streptomycin and the BCA kit were purchased from Beyotime Biotechnology. AK (cat. no. A113942) was purchased from Shanghai Aladdin Biochemical Technology Co., Ltd. D-(+)-Glucose was purchased from Shanghai HuSHI Co., Ltd. Insulin was purchased from Shanghai Fosun Pharmaceutical (Group) Co., Ltd. A sterile BSA-coupled free fatty acid (FFA) mixture solution was obtained from Shanghai Siduorui Biotechnology Service Co., Ltd. The PPARα agonist fenofibrate was acquired commercially from MedChemExpress. The PPARα agonist Wy-14,643 was purchased from Shanghai Aladdin Biochemical Technology Co., Ltd. The PPARα antagonist GW6,471 was acquired commercially from MedChemExpress. Antibodies against β-Tubulin (cat. no. 80713-1-RR), TAS1R2 (cat. no. 29344-1-AP) and PLCβ (cat. no. 66668-1-Ig) were purchased from Wuhan Proteintech Group, Inc. Antibodies against G protein subunit alpha transducin 3 (GNAT3; cat. no. A15982), p-PLCβ (cat. no. AP0837) and TAS1R3 (cat. no. A10157) were purchased from Wuhan ABclonal Biotech Co., Ltd. The antibody against diacylglycerol kinase eta (DGKH; cat. no. AF0611) was purchased from Affinity Biosciences. Detailed information regarding the product brands, dilution ratios, and catalog numbers for all antibodies can be found in Table SI.

Determination of the AK administration. A concentration of 2 mg/ml AK in drinking water was used, this was determined by converting the human ADI (15 mg/kg/day) to a mouse equivalent dose (27). Using the formula HED=human dose x [Km human/Km mouse] (Km human=37, Km mouse=3), the mouse ADI was calculated as 185 mg/kg/day. Based on the measured water intake of the mice on HFD (100-140 ml/kg/day), a concentration range of 1.32-1.85 mg/ml was calculated. Finally, 2 mg/ml was used to ensure effective exposure while keeping close to human ADI.

Animals and treatments. Wild-type (WT) and PPARα-null (KO) mice (129/Sv strain) were obtained from Dr Frank J. Gonzalez at the National Cancer Institute, Bethesda, MD, USA (28), and subsequently bred in-house at Ningbo University. A total of 88 healthy 6-week male mice were used for the 3 experiments mentioned below. The mean body weights were 18.0±0.5 g (WT) and 17.8±0.6 g (KO) before the experiment. The mice

were housed in individual ventilated cages under controlled humidity (60±5%) and temperature (24±1˚C) and a 12/12-h dark/light cycle. The mice were monitored daily for general health (activity, posture, fur condition, food/water intake) by trained staff. On the terminal procedure day, monitoring was continuous from carbon dioxide inhalation until confirmation of death. The animal procedures were approved by the Animal Ethics and Welfare Committee of Ningbo University (approval no. AEWC-NBU20230140; Ningbo, China).

In the first experiment, 10 WT mice were randomly divided into WT group (n=5) and WT-AK group (n=5). Another 10 KO mice were divided into the KO group (n=5) and the KO-AK group (n=5). The sample size design followed previous study and the 3R framework (29). A randomization table was utilized to assign experimental groups, with all procedures executed by an independent technician blinded to the animal handling. All the mice were fed a 60% HFD, and those in the WT-AK and KO-AK groups were treated with an additional 2 mg/ml AK in drinking water. Food and water were replaced every 48-72 h to keep them fresh. Food and water intake were recorded to track metabolic changes. After 11 weeks of treatment, oral glucose tolerance test (OGTT) and insulin tolerance test (ITT) were performed with a 3-day interval.

In a second experiment, 25 WT and 25 KO mice were divided into the control (CON) group, F5, F25, F125 and Wy (n=5), where they were treated with 5, 25 or 125 mg/kg fenofibrate (F5, F25or F125, respectively) twice a day and with 160 mg/kg Wy-14,643 once a day by oral gavage for 5 days to explore the direct regulatory effects of PPARα on the STR signaling pathway. All the drugs were suspended in 1% (w/v) sodium carboxymethylcellulose solution before administration. The CON groups were administered the same volume of vehicle during this period.

In a third experiment, 9 WT and 9 KO mice were allocated to 6 groups: WT, WT-AK, WT-AK-F, KO, KO-AK, and KO-AK-F (n=3). All the mice were fed a 60% HFD, and those in the WT-AK, WT-AK-F, KO-AK and KO-AK-F groups were treated with an additional 2 mg/ml AK in drinking water. After 10 weeks of treatment, the WT-AK-F and KO-AK-F groups were treated with 25 mg/kg fenofibrate twice daily via oral gavage for 2 weeks to investigate whether PPARα activation attenuates hepatic steatosis by inhibiting the STR signaling. The fenofibrate was dissolved in 1% (w/v) sodium carboxymethylcellulose solution before administration. The remaining groups were administered the vehicle during this period. The dosage and regimen of fenofibrate were selected based on a previously study that could effectively inhibit NAFLD development (30).

All mice were sacrificed at the scheduled experimental endpoint. The mice were individually placed in a transparent induction chamber prefilled with ambient air. Medical-grade carbon dioxide (CO_2) was introduced at a controlled flow rate (20-30% of the chamber volume per minute), resulting in a gradual increase in CO_2 concentration and loss of consciousness. While the animal remained unconscious, terminal blood collection was performed as part of the procedure. CO_2 exposure was then increased to a higher concentration (~70%) and maintained until complete respiratory arrest, which was sustained for an additional 5 min. Mortality was verified by the absence of respiration and cardiac activity and subsequently confirmed by cervical dislocation. No unscheduled mortality occurred prior to the endpoint. After cervical dislocation, liver tissues were collected. The blood samples were centrifuged at 800 x g for 15 min at 4˚C. The serum was cryopreserved at -20˚C for analysis within 3 days. After being scaled, half of the biggest lobe was fixed in 10% neutral formalin at room temperature for 24 h, and the remaining tissues were stored at -80˚C.

OGTT. After the 11-weeks of treatment, all the mice (WT, WT-AK, KO, and KO-AK groups) in experiment 1 were fasted for 12 h and gavaged with a glucose solution (2.5 g per kg body weight). Blood glucose levels were measured at 0, 30, 60, 90, and 120 min using a glucometer (ONETOUCH Verio; LifeScan, Inc.) following tail-tip blood sampling. Blood (5-10 μl) was collected at each predefined time point using a sterile lancet. During the fasting period, the mice were allowed to drink control water to eliminate potential AK-induced disturbances in insulin and gastrointestinal hormone secretion (31). The area under the curve (AUC) was calculated to assess glucose tolerance.

ITT. For ITT, the WT and WT-AK mice in experiment 1 were fasted for 6 h, followed by intraperitoneal injection of insulin (0.8 U/kg body weight). After insulin injection, the blood glucose levels were measured at 0, 15, 30, 45 and 60 min using a glucometer. Blood sampling and glucose measurement were performed using the same method and sampling volume as those used in the OGTT. Blood glucose concentrations over time were plotted as a glucose-time curve and the AUC was calculated to compare the insulin sensitivity.

Cellular experiments. Hepa1-6 cells (Suzhou Hysigen Bioscience Co., Ltd.) and Huh-7 cells (Wuhan Pricella Biotechnology Co., Ltd.) were cultured in high-glucose DMEM (4.5 g/l; Corning Life Sciences) supplemented with 10% fetal bovine serum and 1% penicillin-streptomycin. These two cell lines were treated with 0.2 mM FFA for 48 h to induce lipid accumulation. Simultaneously, AK (0, 1, 3, 10 and 20 mM) was added to the aforementioned growth media to explore the effects of AK on lipid accumulation. 50% AK was added and the incubation continued for 48 h. The TG content of the cells was measured following the procedures described below.

Knock-down and inhibition of PPARα. A second-generation lentiviral packaging system was used in this experiment. Lentiviral particles were packaged in 293T cells (ATCC) and produced in 293T cells (ATCC) by co-transfection with 8 μg shRNA plasmid, 6 μg packaging plasmid (Δ8.2) and 4 μg envelope plasmid (VSV-G). Lentiviral supernatants were collected at 48 h post-transfection, filtered through a 0.45-μm filter, and used to infect Hepa1-6 cells at a multiplicity of infection of 10. Hepa1-6 cells were passaged into 10-cm dishes 24 h before infection. A total of 10 ml of DMEM containing lentivirus packaged with short hairpin (sh) NC and sh*Pparα* (Wuhan Miaoling Biotechnology Co., Ltd.) plasmids was added to DMEM at a 1:1 ratio during the medium change. At 24 h after infection, the culture medium containing the lentivirus was discarded and replaced with fresh medium. Finally, the infected cells were selected using DMEM supplemented with 30 μg/ml blasticidin (Beyotime Biotech Inc.) for 48 h and maintained

in medium containing 3 μg/ml blasticidin to purify stable transfectants. Successful gene knockdown was confirmed by reverse transcription-quantitative (RT-q) PCR and western blot analysis. Hepa1-6 cells induced by FFA were co-treated with 2 μM GW6,471 or AK (0, 1, 3, 10 and 20 mM) for 48 h.

The shNC plasmid was obtained from Wuhan Miaoling Biotechnology Co., Ltd. (cat. no. P47365). The sh*Pparα* sequences were as follows: sh*Pparα*-1: 5'-AAGAATTCTTAC AAGAAAT-3'; sh*Pparα*-2: 5'-GGAAAGTCCCTTATCTGA AT-3'; sh*Pparα*-3: 5'-GAACATCGAGTGTCGAATAT-3'.

Measurement of TC and TG concentrations. The TC and TG concentrations in the plasma and liver tissues were determined using commercially available TC and TG assay kits. The liver tissues were weighed and homogenized with 9 volumes of saline. For analysis, 2 μl aliquots of plasma or liver homogenate samples were combined with 67 μl of reagent R1. After 5 min of incubation at 37˚C, the absorbance was measured at the appropriate wavelengths (TC; 546 and 660 nm; TG; 546 and 700 nm). After 33 μl of reagent R2 was added, the samples were incubated for another 5 min. The absorbance was measured at the aforementioned wavelengths following the manufacturer's protocol.

Measurement of liver glycogen concentration. Concentrations of glycogen in liver tissues were determined using a commercially available glycogen assay kit (cat. no. A043-1-1; Nanjing Jiancheng Bioengineering Institute). The weighed liver tissue was boiled in a metal bath at 100˚C after adding 3-fold volumes of the alkaline solution. Glycogen chromogenic solution and double-distilled water were added. The mixture was boiled again and then transferred to a 96-well plate for absorbance measurement at 620 nm.

Measurement of liver DAG. The hepatic DAG levels were quantified using a commercial ELISA kit (cat. no. KX30762; Shanghai Yaxin Biotechnology Co. Ltd.). The liver tissues were homogenized in ice-cold saline at 4˚C. The homogenates were centrifuged at 1,200 x g for 15 min at 4˚C. Following the procedures in the kit, the homogenate DAG concentrations were measured and normalized.

Histopathological analysis. Fresh liver tissues were fixed in 10% neutral formalin at room temperature for 24 h. The tissues were then dehydrated in a serial concentration of ethanol (70, 80, 90 and 100%). After clearing with xylene, the tissues were embedded in paraffin and serial 4 μm sections were prepared. To detect polysaccharide content, the liver sections were deparaffinized and stained at room temperature by oxidation with 0.5% periodic acid for 8 min, followed by Schiff reagent incubation for 15 min and H&E counterstaining for 2 min. Representative images were captured using a light microscope (Olympus BX43; Olympus Corporation). Pathological analysis was carried out by a certified pathologist unaware of the study design.

Oil Red O staining. Hepa1-6 and Huh-7 cells were washed twice in PBS and then fixed in 10% neutral formalin buffer for 30 min at 4˚C. The cells were stained with fresh oil red O working solution for 30 min, soaked in 60% isopropyl alcohol for 10 sec and finally stained with hematoxylin for 2 min at room temperature. Lipid droplet formation in cells was visualized via inverted phase-contrast microscopy (Olympus CKX41; Olympus Corporation).

RT-qPCR analysis. Frozen liver and adipose tissues were lysed in TRIzol® (Invitrogen; Thermo Fisher Scientific, Inc.) and homogenized using a MagNA Lyser (Roche Diagnostics). The RNA concentration was quantified spectrophotometrically, with purity assessed using the OD_{260}/OD_{280} absorbance ratio. Total RNA (1 μg) from the liver sample was subjected to reverse transcription in a reaction volume of 20 μl following the manufacturer's protocol of ABScript III RT Master Mix for qPCR (cat. no. RK20428; ABclonal Biotech Co., Ltd.). The synthesized cDNA was stored at 20˚C until analysis. The primer sequences are listed in Table SII. Q-PCR amplification on 96-well plates was performed in a 10-μl incubation containing 1 μl cDNA, 5 μl UltraSYBR Mixture, 0.4 μl primer, and 3.6 μl purified water using a LightCycler 480II (Roche Diagnostics). The thermocycling conditions were set as initial denaturation at 95˚C for 5 min, followed by 40 cycles of 95˚C for 10 sec and 60˚C for 30 sec. The $2^{-\Delta\Delta Cq}$ method was used to quantify the expression of target genes (32). The measured mRNA abundance was normalized to that of GAPDH and expressed as a fold change equivalent to that of WT control mice. All experiments were independently repeated at least three times.

Western blot analysis. Frozen liver tissues were homogenized in 9 volumes of RIPA lysis buffer (Suzhou NCM Biotech Co., Ltd.) containing 1% PMSF and 1% protein phosphatase inhibitor). The supernatants were collected by centrifugation at 15,000 x g for 15 min at 4˚C. Protein concentrations were determined using a BCA protein assay kit (cat. no. B610409; Suzhou NCM Biotech Co., Ltd.). Equal amounts of protein (30 μg per lane) were mixed with 5X SDS-PAGE loading buffer (Beyotime Biotech Inc.) and boiled for 8 min. The 10% SDS polyacrylamide gels were separated for 1 h. The proteins were transferred to 0.45-μM PVDF membranes for 1.5 h in an ice bath. All membranes were blocked with 5% skimmed milk at room temperature for 3.5 h. Subsequently, the membranes were incubated with primary antibodies at 4˚C overnight. After three 10-min washes with TBS-0.1% Tween-20, the membranes were incubated with HRP-conjugated secondary antibodies for 2 h at room temperature (primers in Table SI). Finally, the ECL substrate was added to the blotted PVDF, and images were recorded using a chemiluminescent imaging system, ChemiScope 6100 Touch (Clinx Science Instruments Co., Ltd.). Densitometric analysis was performed using ImageJ (version 1.53; National Institutes of Health).

RNA sequencing (RNA-seq) analysis. The liver samples from 4 groups (WT-CON, WT-Wy, KO-CON and KO-Wy; n=3/group) in cohort 2 were analyzed. Total RNA was extracted using Trizol reagent (cat. no. B610409; Sangon Biotech Co., Ltd.), treated with DNase I, and assessed for integrity (RIN >8) and purity using a NanoPhotometer spectrophotometer (Implen GmbH) and a Qubit fluorometer (Thermo Fisher Scientific, Inc.). The sequencing libraries were prepared using the VAHTS mRNA-seq V2 Kit (cat. no. NR612-01; Vazyme Biotech Co., Ltd.) for Illumina, including poly-A mRNA

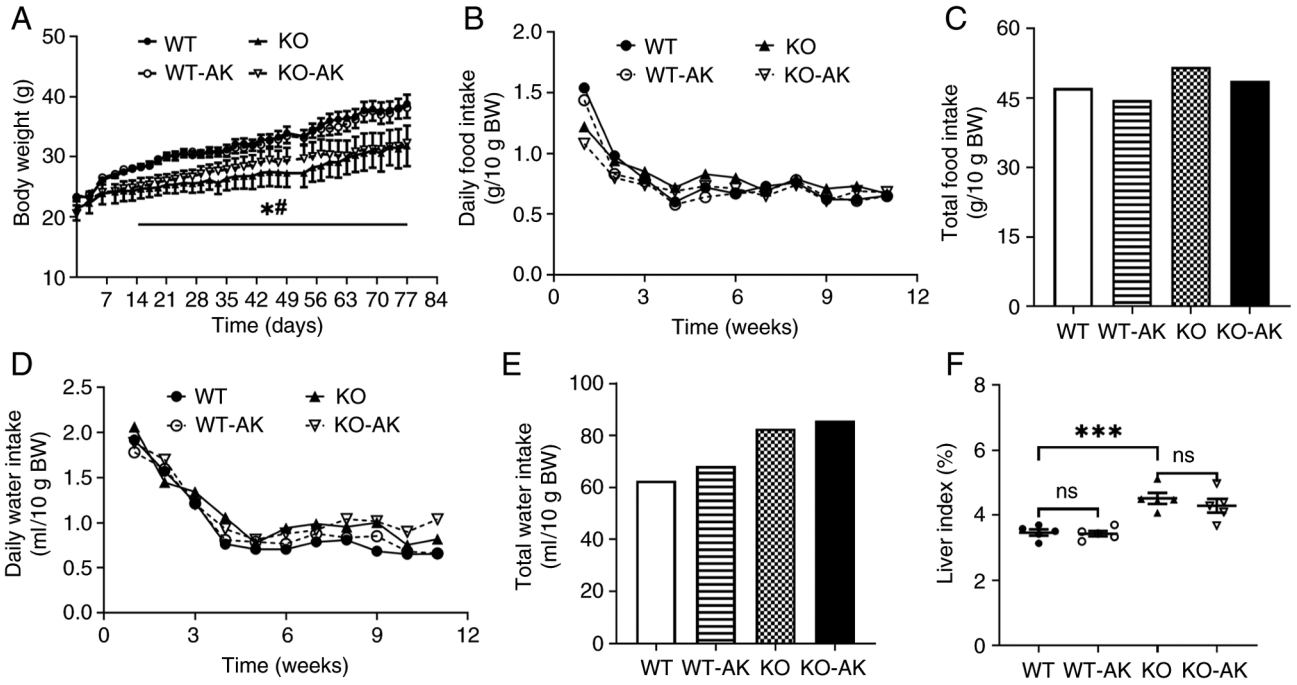

Figure 1. AK intake does not modify the phenotype of the WT or KO mice. (A) Body weight gain of the WT and KO mice. (B) Cumulative food intake of the WT and KO mice. (C) Ratio of total food intake to body weight per 10 g in the WT and KO mice. (D) Cumulative water intake of the WT and KO mice. (E) Ratio of total water intake to body weight per 10 g in the WT and KO mice. (F) Liver indices of the WT and KO mice. The data were expressed as the means ± SEM. *P<0.05 and ***P<0.0001 WT vs. KO mice; #P<0.05 WT-AK vs. KO-AK mice; ns. not significant. Differences at the time points were determined by two-way ANOVA and Bonferroni post hoc correction. AK, acesulfame-K; BW, body weight; KO, PPARα-null; WT, wild-type; PPARα, peroxisome proliferator-activated receptor α.

enrichment, fragmentation (150-200 bp), RT, adapter ligation, and PCR amplification. Paired-end RNA sequencing (150 bp reads) was performed on an Illumina NovaSeq platform (Illumina, Inc.). The final libraries were quantified using a Qubit fluorometer and Agilent Bioanalyzer and loaded onto the sequencer at a final concentration of 10 pM. The raw reads were filtered using Trimmomatic (version 0.39; https://github.com/usadellab/Trimmomatic) with Q≥20, aligned to the mouse reference genome (GRCm38) using HISAT2 (version 2.2.1; https://daehwankimlab.github.io/hisat2), and quantified as transcripts per million (TPM) using StringTie (version 2.1.4; https://ccb.jhu.edu/software/stringtie). Differentially expressed genes [|FC|≥1.5, False Discovery Rate (FDR) <0.01; DESeq2], including *Acot1*, *Ehhadh*, and *Dgkh*, were validated by qPCR (primers in Table SII).

Statistical analysis. All experimental subjects were retained for statistical evaluation. Parametric distribution assumptions were confirmed, with results reported as mean ± SEM. Between-group differences were assessed using two-tailed Student's t tests following verification of variance homogeneity. Multigroup comparisons employed one-way ANOVA with Bonferroni adjustment for homogeneous datasets, whereas heteroscedastic data were analyzed through Welch's ANOVA followed by Tamhane's T2 post hoc testing. Statistical significance threshold was set at α=0.05. A post hoc statistical power analysis was performed for the comparisons of liver TG content in experiment 3. Based on the experimentally observed effect sizes, the actual sample size (n=3 per group), and a two-tailed significance level (α) of 0.05, the statistical power was calculated for the comparison between WT-AK and WT-AK-F group. The liver TG content in the WT-AK-F group was significantly lower than that in the WT-AK group [(Mean difference)=3.504-5.532=-2.028 μg/mg; P<0.05]; two-tailed unpaired t-test. The magnitude of this difference was quantified as Cohen's d=8.50, 95% CI [3.0, 14.0]. Analytical procedures were executed in GraphPad Prism 9.5.1 (Dotmatics). P<0.05 was considered to indicate a statistically significant difference.

Results

Chronic AK consumption promotes NAFLD without altering the phenotype. After 12 weeks of HFD treatment, the WT mice exhibited markedly greater body weight gain compared with the KO mice (Fig. 1A). AK supplementation failed to induce significant changes in body weight gain in either mouse line (Fig. 1A). The WT and the KO mice that consumed AK both presented a reduction in food intake but an increase in water consumption (Fig. 1B-E). The liver weight was markedly higher in the KO mice compared with the WT mice, but AK supplementation did not cause an increase in liver weight in either group (Fig. 1F). These data suggested that AK administration did not affect metabolic phenotype in either the WT mice or the KO mice.

A 12-week HFD regimen induced differential hepatic lipid accumulation between two mouse lines, as indicated by H&E-stained samples in Fig. S1A-D. AK exacerbated hepatic steatosis in the WT mice but not in the KO mice (Fig. 2A). The plasma ALT and AST levels were not altered by AK in either the WT or KO mice (Fig. S2A and B). No significant change in mRNA expression levels of inflammatory genes was visible upon AK treatment in the WT mice, whereas

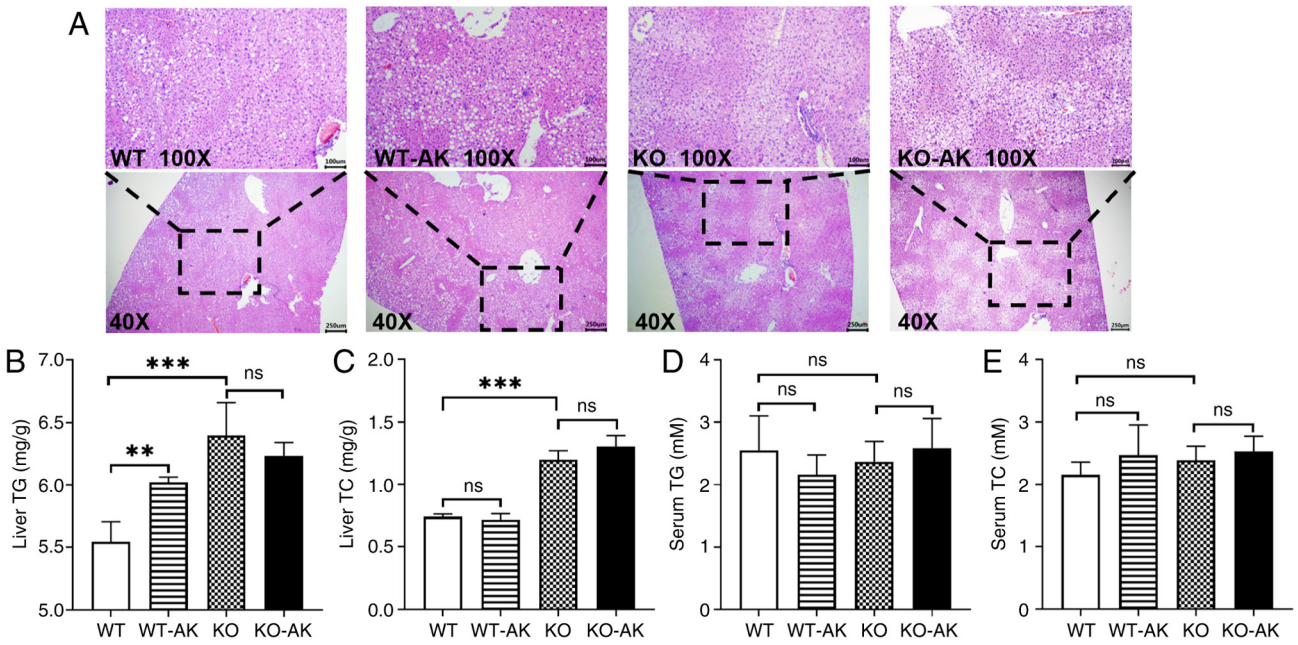

Figure 2. AK promotes NAFLD development in the WT mice not the KO mice. (A) Hematoxylin and eosin staining of liver tissues from each group (magnification, x40 and x100). (B) Liver TG and (C) TC concentrations in each group. (D) Serum TG and (E) TC concentrations in each group. The data were expressed as the means ± SEM. **P<0.01, ***P<0.0001, ns. not significant. AK, acesulfame-K; NAFLD, nonalcoholic fatty liver disease; WT, wild-type; KO, PPARα-null; TC, total cholesterol; TG, triglycerides; PPARα, peroxisome proliferator-activated receptor α.

a significant downregulation was observed in the KO mice (Fig. S2C-F). Moreover, AK supplementation increased the hepatic TG levels by approximately 10% in the WT mice, whereas no significant change was observed in the KO mice (Fig. 2B). By contrast, the hepatic TC levels were significantly higher in the KO mice than in the WT mice. However, AK supplementation did not significantly affect hepatic TC levels in either mouse line (Fig. 2C). No significant differences were observed in the serum TC or TG concentrations among the 4 groups (Fig. 2D and E). Thus, chronic AK consumption promotes NAFLD development in the WT mice but not in the KO mice.

AK impairs glucose homeostasis via activation PLCβ in STR signaling. After 11 weeks of HFD consumption, an oral glucose tolerance test was performed followed by insulin sensitivity experiments (Fig. 3A). An ~25% higher mean blood glucose peak level was observed in the WT-AK mice as compared with the WT mice (Fig. 3B). AK supplementation impaired glucose tolerance in the WT mice but not in the KO mice (Fig. 3B and C). After the 6-h fasting period, the fasting blood glucose levels of the mice in the KO group were ~25% lower compared with those in the WT group. No significant difference in fasting blood glucose levels was observed between the WT and WT-AK mice (Fig. 3D). AK supplementation did not modify the insulin sensitivity in either the WT mice or the KO mice (Fig. 3E and F). Therefore, AK supplementation may impair the glucose tolerance without altering insulin sensitivity in the WT mice.

Expression of the *Gck* and *G6pc1* genes was markedly upregulated in the WT-AK mice compared with the WT mice (Fig. 3G and H). *Gck* mRNA expression was increased by ~50%, paralleled by a 1-fold increase in *G6pc1* mRNA expression compared with WT mice (Fig. 3G and H). Similarly, the mRNA expression levels of the glucose transport genes *Slc2a2* and *Slc5a10* were markedly lower in the WT-AK mice compared with the WT mice (Fig. 3I and J). The effect on differential gene expression regulation is lost in mice that are depleted of PPARα. Furthermore, in the WT-AK mice, mRNA levels of the fatty acid synthesis genes *Acaca* and *Elovl6* were higher compared with those in the WT mice, whereas no significant differences were found in the expression of lipid and glycogen metabolism genes (Fig. S3A-H).

Periodic acid-Schiff staining of liver sections revealed more pronounced glycogen deposition in the WT-AK mice compared with in the WT mice (Fig. 3K). The liver glycogen content was elevated by 25% in the WT-AK mice compared with the WT mice, whereas the effect was lost in the KO mice (Fig. 3L). Compared with that in WT-AK mice, the expression of phosphorylated PLCβ in WT-AK mice was elevated, suggesting the activation of STR signaling (Fig. 3M). Although the downregulation of TAS1R2 and TAS1R3 expression was also observed in the WT-AK group, they were supposed to be adaptive modifications. However, none of the aforementioned modifications were observed between the KO and KO-AK mice (Fig. 3M). Therefore, physiologically, PPARα mediates the disruption of glycolipid metabolism by AK in the liver by activating STR signaling, especially by increasing the phosphorylated PLCβ.

AK-increased lipid accumulation via PLCβ is dependent on PPARα. Oil Red O staining revealed a dose-dependent increase in lipid accumulation in both Hepa1-6 and Huh-7 cells treated with increasing AK concentrations (Fig. 4A). Supporting results were obtained by direct measurement of the TG contents in both cell lines (Fig. 4B and C). In the Hepa1-6 cell line, the addition of 10 mM AK led to a

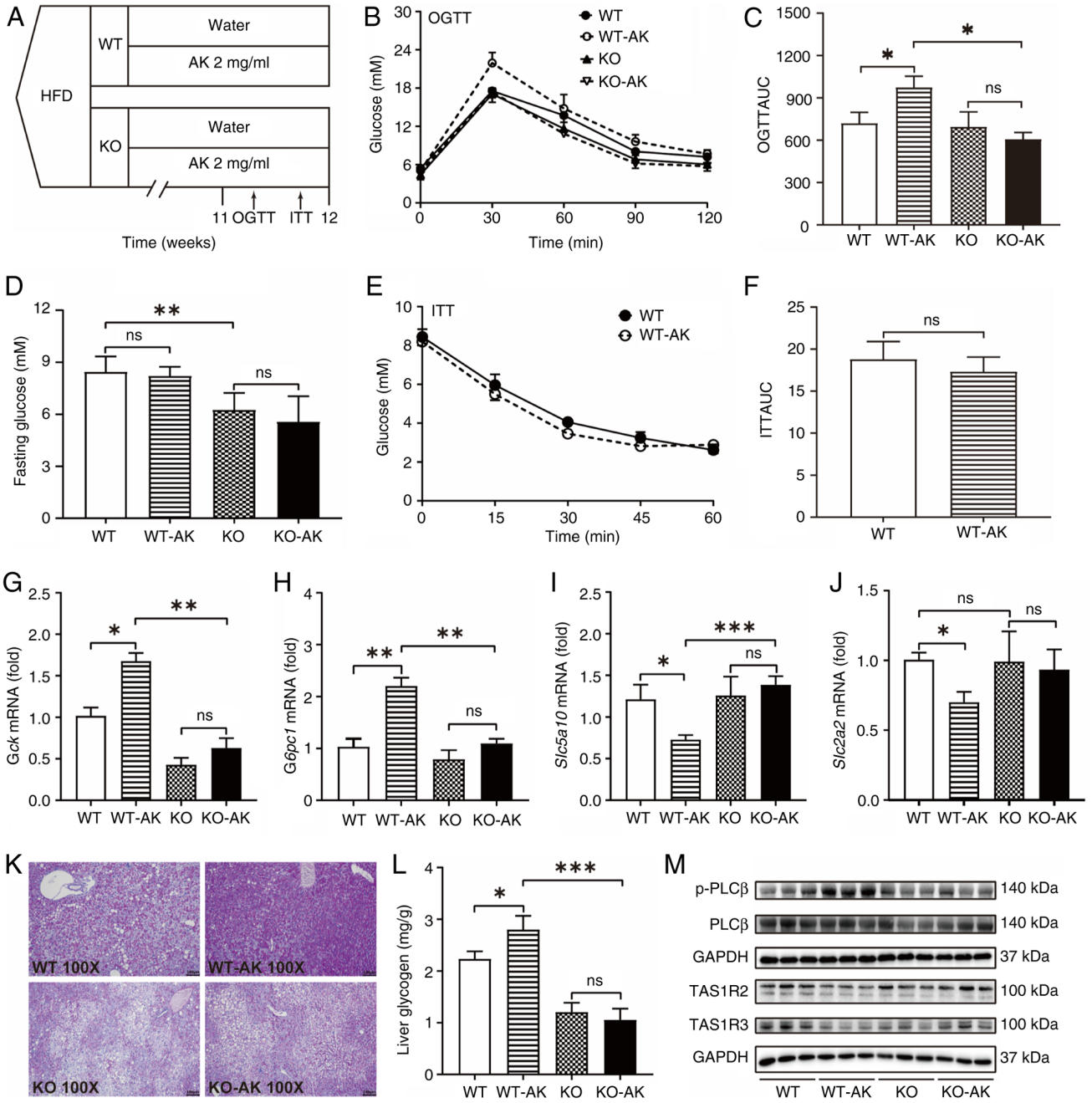

Figure 3. AK impairs glucose homeostasis via activating hepatic PLCβ in STR signaling. (A) HFD-fed WT and KO mice receiving normal water or AK supplementation (12-week intervention, n=5). Metabolic tests (OGTT/ITT) at weeks 11-12. (B) OGTT and (C) the corresponding AUCs in each group. (D) Fasting blood glucose levels in the different groups of mice after 6 h of fasting. (E) ITT and (F) the corresponding AUCs in the WT and WT-AK mice. The average changes in (G) *Gck*, (H) *G6pc1*, (I) *Slc2a2* and (J) *Slc5a10* transcription in the 4 groups. (K) PAS staining of liver tissues from each group (magnification, x100). (L) Liver glycogen content in each group. (M) Liver protein expression levels of PLCβ, p-PLCβ, TAS1R2, and TAS1R3 were measured using western blot analysis. The data were expressed as the means ± SEM. *P<0.05, **P<0.01, ***P<0.0001, ns. not significant. AK, acesulfame-K; p-, phosphorylated; PLCβ, phospholipase C beta; STR, sweet taste receptor; HFD, high-fat diet; WT, wild-type; KO, PPARα-null; OGTT, oral glucose tolerance test; ITT, insulin tolerance test; AUC, area under the curve; *G6pc1, glucose-6-phosphatase catalytic subunit 1*; *Gck, glucokinase*; *Slc2a2, solute carrier family 2, member 2; Slc5a10, solute carrier family 5, member 10*; TAS1R, taste 1 receptor member.

concentration-dependent increase in PLCβ phosphorylation during treatment (Fig. 4D). A comparable activation of PLCβ was also observed when the same concentrations of AK were added to Huh-7 cells (Fig. 4E).

To functionally prove the involvement of PPARα in the observed AK effects, Hepa1-6 cells were transfected with three sh*Pparα* plasmids via lentiviral infection (Fig. 5A). PPARα protein expression was downregulated in sh*Pparα*-2-transfected Hepa1-6 cells, as confirmed by western blot analysis (Fig. 5B). No increase in PLCβ phosphorylation was observed in sh*Pparα*-transfected Hepa1-6 cells despite exposure to increased AK concentrations (Fig. 5C). Oil Red O staining and intracellular TG analysis revealed that lipid accumulation in sh*Pparα*-2-transfected cells was not increased by serially increased concentrations of AK (Fig. 5D and E). Similarly to the knock-down experiment, both the PLCβ

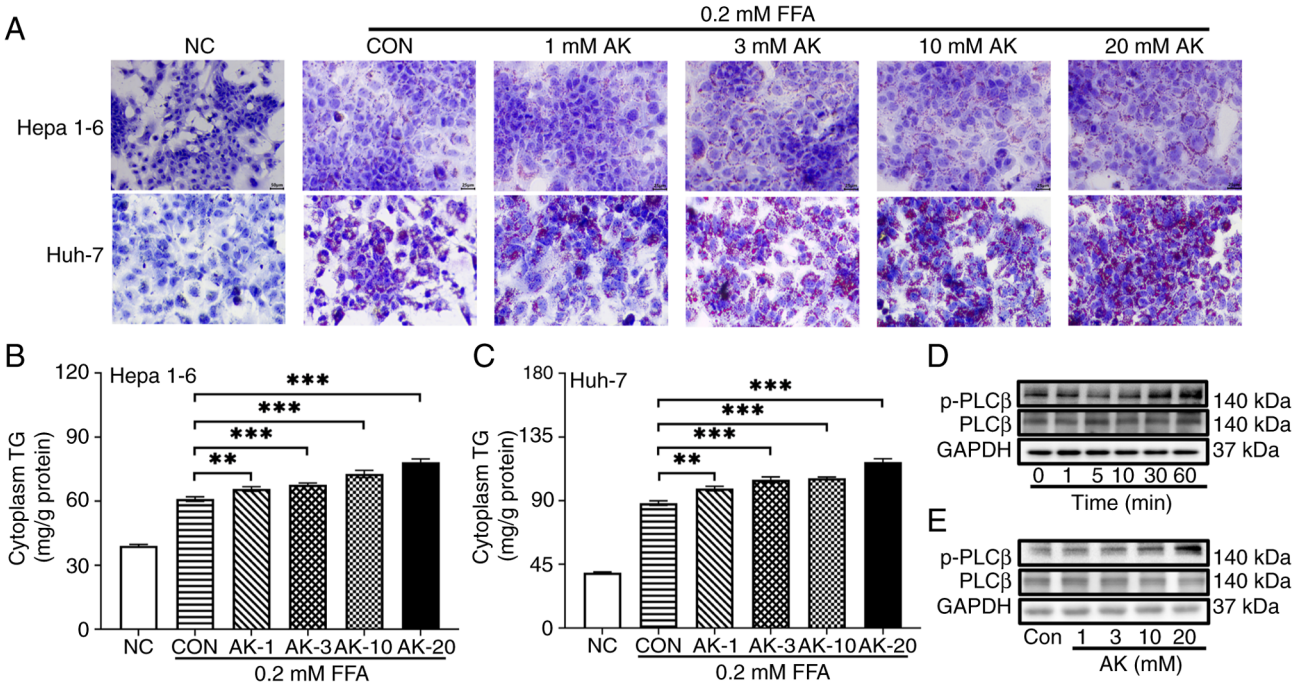

Figure 4. PLCβ is activated in lipid accumulation increased by AK in Hepa1-6 and Huh-7 cells. (A) Oil Red O staining of Hepa1-6 and Huh-7 cells after 48 h of treatment with FFA combined with AK. (B) TG content in the cytoplasm of Hepa1-6 cells. (C) TG content in the cytoplasm of Huh-7 cells. (D) PLCβ phosphorylation in Hepa1-6 cells during a time course of AK treatment. (E) PLCβ phosphorylation in Hepa1-6 cells after 1 h of AK treatment. The data were expressed as the means ± SEM. **P<0.01, ***P<0.0001. PLCβ, phospholipase C beta; AK, acesulfame-K; Hepa1-6, mouse hepatoma cells; Huh-7, human hepatocellular carcinoma cells; FFA, free fatty acid; TG, triglycerides; WT, wild-type; NC, control group without free fatty acid treatment; CON, control group without added acesulfame-K but with free fatty acids added; KO, PPARα-null; p-, phosphorylated.

activation and the lipid accumulation in AK treatment were also abolished by GW6,471, a selective PPARα antagonist (Fig. 5F and G). Accordingly, lipid accumulation in hepatocytes and the activation of STR signaling component PLCβ is dependent on PPARα.

Multiple targets of the hepatic STRs including PLCβ are regulated by PPARα. Next, the effects of PPARα on the STR signaling pathway were explored in mice treated with increasing doses of fenofibrate and Wy-14,643, a more selective PPARα agonist. The mRNA expression levels of the PPARα target genes *Acot1* and *Ehhadh* increased progressively with increasing doses of the PPARα agonist in the WT mice. Such a dose-dependent effect was not detected in the KO mice (Fig. 6A and C). The two mouse lines presented distinct responses to PPARα activation, where the TAS1R2 level increased and the TAS1R3 level progressively decreased (Fig. 6B). GNAT3, the α subunit of the taste receptor G protein involved in intracellular taste signaling, was progressively downregulated upon PPARα activation (Fig. 6B). The activation of GNAT3 facilitated PLCβ-mediated hydrolysis of phosphatidylinositol 4,5-bisphosphate, while PLCβ expression was downregulated upon PPARα activation (Fig. 6B). However, the mRNA transcriptions of the aforementioned components were not modified (Fig. S4A and B). In contrast to the results from the WT mice, the aforementioned modifications of the STR signaling components were absent in the KO mice (Fig. 6D).

Dgkh, a key regulator of DAG catabolism, was identified as the only upregulated gene among the 10 DAG kinase family members analyzed, within the subset of 1,731 genes markedly upregulated by PPARα agonist treatment (Fig. 6E and F). The mRNA expression level of *Dgkh* exhibited a dose-dependent increase in the WT mice following treatment with Wy14,643 (Fig. 6G). Similarly, the DGKH level was upregulated by the activation of PPARα, which did not occur in KO mice (Fig. 6H and I). A markedly increased expression level of hepatic DAG was observed in the KO mice compared with the WT mice (Fig. 6J). Therefore, PPARα regulates more targets of the STR signaling besides the PLCβ, including TAS1R2, TAS1R3, and DGKH.

Activated PPARα meliorates AK-induced NAFLD by inhibiting hepatic PLCβ. The therapeutic action of pharmacologically activated PPARα in AK-induced NAFLD was designed as shown in the flow chart (Fig. 7A). Consistent with the aforementioned observations, hepatic steatosis was markedly exacerbated in the WT-AK mice compared with the control mice. AK-induced lipid accumulation was effectively rescued in the WT-AK-F mice through pharmacological challenge with fenofibrate (Fig. 7B). In the KO mice, neither the pro-steatotic effect of AK nor the therapeutic response to fenofibrate was observed, suggesting both a physiological and pharmacological role of PPARα (Fig. 7B). Hepatic TG content was elevated by 10% in the WT-AK mice compared with the control group. Fenofibrate challenge led to a sharp reduction in this lipid marker compared with that in WT-AK and this was only observed in the WT mice (Fig. 7C). In the KO mice, no increase in TG by AK or decrease in TG by fenofibrate was observed (Fig. 7C).

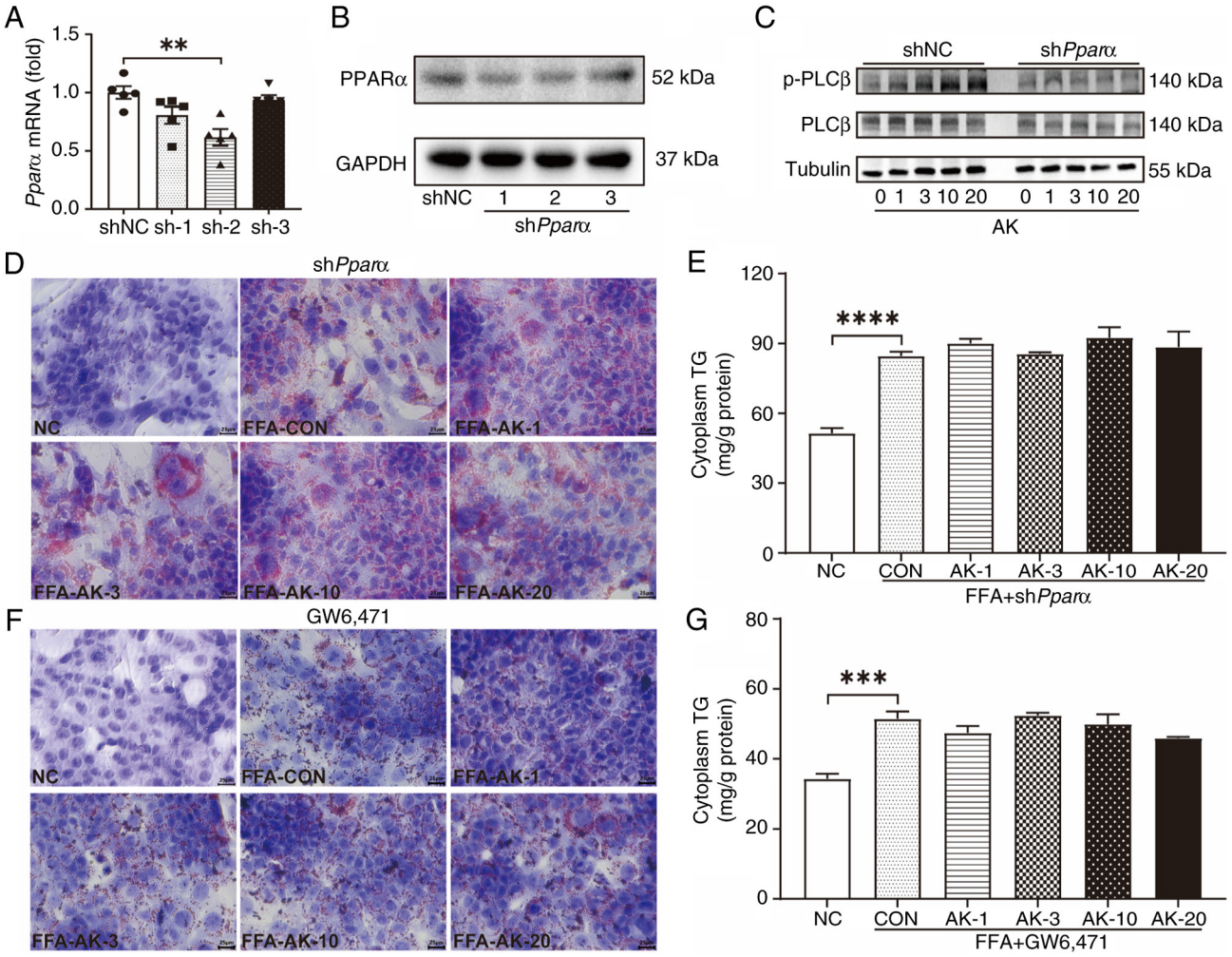

Figure 5. PLCβ activation and lipid accumulation induced by AK are deleted by PPARα downregulation. (A) *Pparα* mRNA levels in Hepa1-6 cells transfected with a vector plasmid and three sh*Pparα* plasmids. (B) PPARα protein levels in Hepa1-6 cells transfected with a vector plasmid and three sh*Pparα* plasmids. (C) PLCβ phosphorylation in Hepa1-6 cells transfected with sh*Pparα*-2 after 1 h of AK treatment. (D) Oil Red O staining of Hepa1-6 cells after transfection with the sh*Pparα*-2 plasmid. (E) TG content in the cytoplasm of Hepa1-6 cells transfected with the sh*Pparα*-2 plasmid. (F) Oil Red O staining of Hepa1-6 cells treated with GW6,471. (G) TG concentration in Hepa1-6 cells treated with GW6,471. The data were expressed as the means ± SEM. **P<0.01, ***P<0.001, ****P<0.0001. AK, acesulfame-K; PLCβ, phospholipase C beta; PPARα, peroxisome proliferator-activated receptor α; sh, short hairpin; Hepa1-6, mouse hepatoma cells; TG, triglycerides; CON, control group without added acesulfame-K but with free fatty acids added; FFA, free fatty acid; GW6,471, a peroxisome proliferator-activated receptor α inhibitor; KO, PPARα-null; NC, control group without free fatty acid treatment; p-, phosphorylated; shNC, short hairpin RNA negative control; TC, total cholesterol; WT, wild-type.

In western blot analysis, a significant elevation of phosphorylated PLCβ expression was observed in the WT-AK mice compared with the control group (Fig. 7D). In the WT-AK-F group, both the total PLCβ and the phosphorylated PLCβ were markedly reduced (Fig. 7D). Notably, neither expression levels of phosphorylated nor total PLCβ was modified in the KO mice (Fig. 7D). These data suggested the steatotic effect of PLCβ activation mediated by physiological PPARα was inhibited by pharmacologically activated PPARα.

Discussion

NNSs are conditionally endorsed by major health authorities as short-term sugar substitutes for weight management. NNS substitution for dietary sugars promotes weight reduction in overweight populations with ad libitum feeding patterns (33). In the present study, the mice ingested an average daily dose of 12 mg/kg AK (converted by the body surface area formula). No changes in body weight gain or biochemical markers were induced by AK treatment. However, marked lipid vacuolization was induced with elevated hepatic triglyceride deposition. Therefore, hepatic metabolic dysregulation was latently induced by chronic AK intake. Based on these data, the potential hepatometabolic risks of chronic NNS consumption should be fully addressed to ensure the health of the public.

Mechanistically, NNSs modulate pancreatic β-cell function through STR-mediated potentiation of insulin secretion (31). Chronic NNS exposure disturbs hepatic insulin signaling through chronic hyperinsulinemia, thereby accelerating glycogen deposition while promoting hepatic lipid storage (34). AK enhances intestinal glucose uptake by activating STRs in the small intestine (35,36). Consequently, the pathogenesis of AK-induced glucose intolerance likely stems from enhanced intestinal absorption of dietary carbohydrates. Glycogen saturation redirects excess glucose into

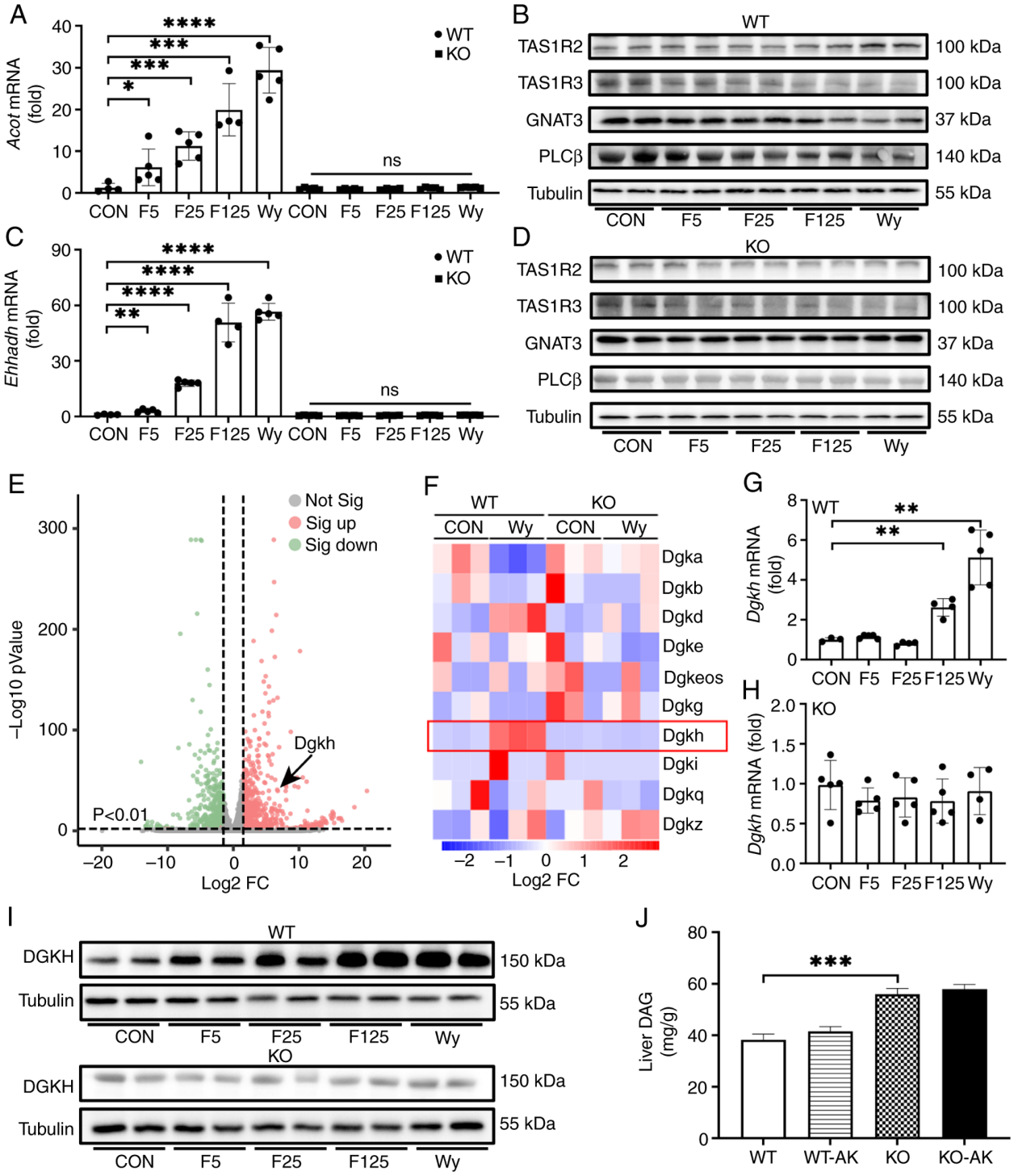

Figure 6. Multiple targets including PLCβ in STR signaling are regulated by PPARα. Upregulation of PPARα target genes (A) *Acot1* and (C) *Ehhadh* by the agonists fenofibrate and Wy-14,643. (B and D) Pharmacological regulation of TAS1R2, TAS1R3, GNAT3, and PLCβ induced by fenofibrate and Wy-14,643. (E) Volcano plot depicting hepatic transcriptomic profiles of Wy14,643-treated mice vs. vehicle controls. (F) Heatmap of diacylglycerol kinase family genes revealed *Dgkh* as a potential PPARα target gene. (G) DAG levels in the liver of the WT, WT-AK mice were lower than those in the KO and KO-AK mice. (H) *Dgkh* transcription regulated by fenofibrate and Wy-14,643 detected using quantitative PCR. (I) Validation of DGKH expression regulated by PPARα agonists fenofibrate and Wy-14,643. (J) Hepatic DAG content in experimental groups. The data were expressed as the means ± SEM. *P<0.05, **P<0.01, ***P<0.001, and ****P<0.0001. PLCβ, phospholipase C beta; STR, sweet taste receptor; PPARα, peroxisome proliferator-activated receptor PPARα, peroxisome proliferator-act; *Acot, acyl-CoA thioesterase*; *Ehhadh, enoyl-CoA hydratase/3-hydroxyacyl-CoA dehydrogenase*; TAS1R, taste 1 receptor member; GNAT3, G protein subunit alpha transducin 3; Wy, Wy-14,643, a peroxisome proliferator-activated receptor alpha agonist; *Dgkh, diacylglycerol kinase eta*; KO, PPARα-null; DGKH, diacylglycerol kinase η; DAG, diacylglycerol; WT, wild-type; CON, control group; FC, fold change; PLCβ, phospholipase C beta.

lipogenesis, driving hepatic steatosis independent of systemic insulin sensitivity. Fat components, not carbohydrates, served as the primary energy substrate in the present study. Thus, the AK-induced hepatic lipid dysregulation in the present study may have arisen from STR activation, not carbohydrate uptake.

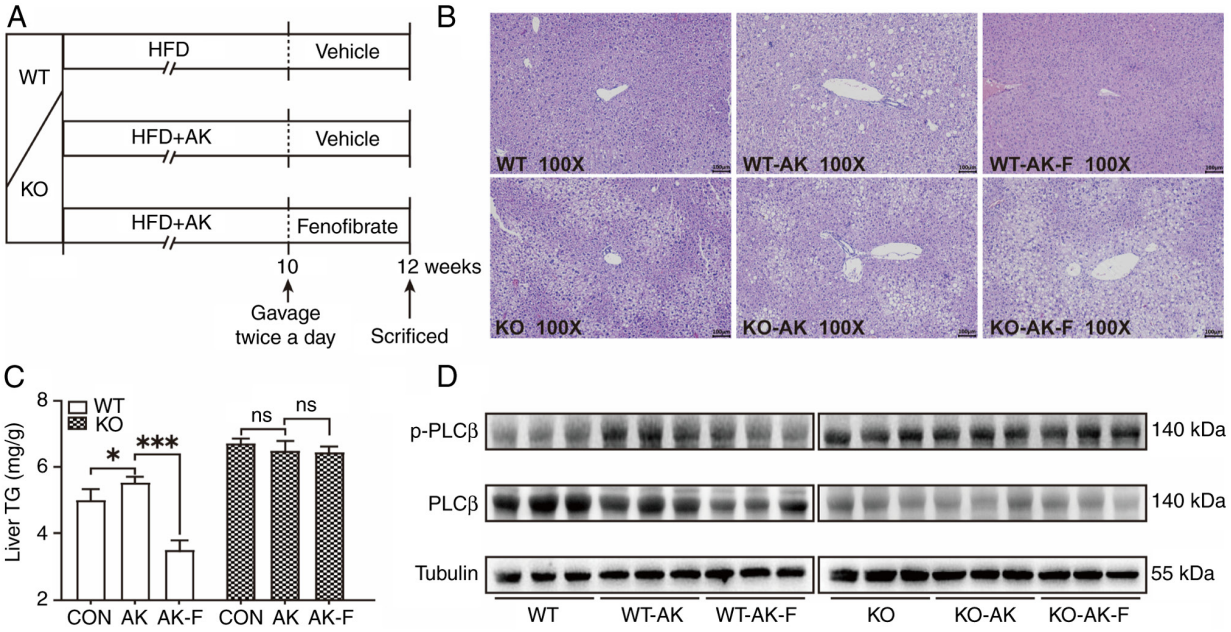

Figure 7. PLCβ is inhibited in steatosis attenuated by pharmacologically-activated PPARα. (A) HFD-fed WT and KO mice receiving normal water or AK supplementation (12-week intervention, n=3). During weeks 16-18, control solvent or F (25 mg/kg) was administered twice daily via oral gavage. (B) Hematoxylin and eosin staining of liver tissues from each group (magnification, x100). (C) Liver TG concentrations in each group. (D) The PLCβ protein expression and phosphorylation status were quantified in each group. Data were expressed as the means ± SEM. *P<0.05, ***P<0.0001, ns. not significant. PLCβ, phospholipase C beta; PPARα, peroxisome proliferator-activated receptor α; HFD, high-fat diet; WT, wild-type; KO, PPARα-null; AK, acesulfame-K; TG, triglycerides; F, fenofibrate; p-, phosphorylated.

PPARα, a key nuclear transcription factor, regulates fatty acid oxidation and ketone body production in liver mitochondria and peroxisomes during fasting (37). PPARα and cyclic AMP responsive element binding protein synergistically regulate gluconeogenic gene expression during fasting (38,39). As previously reported, brief fasting caused a significant decrease of blood glucose level in the KO mice in the present study (39). Considering the risk of shock and adverse responses, the insulin tolerance test was not conducted in the KO mice. Chronic exposure to AK modulated HFD-induced transcriptional adaptation in gluconeogenic pathways, which is strictly dependent on PPARα. The emergence of novel pan-PPAR agonists positions them as a highly promising drug class for NAFLD treatment (40). The present study provided theoretical validation for their clinical application in alleviating diet-induced NAFLD.

In STR signaling, downstream PLCβ activation generates DAG, a second messenger that subsequently activates the PKC family to regulate cellular processes (41,42). In the present study, TAS1R2 and TAS1R3 downregulation after AK challenge was observed. PLCβ phosphorylation was observed in hepatocytes following AK treatment in both *in vivo* and *in vitro* models, indicating AK-induced activation of STR signaling. These events were abolished in the KO mice. Based on these findings, PPARα is supposed to be physiologically involved in activating PLCβ in STR signaling triggered by AK, contributing to metabolic reprogramming in the liver.

Communication between different organelles is facilitated by signaling pathways and membrane contact sites (43). The role of lipids in the morphological and functional regulation of different organelles was highlighted (44). Lipids such as DAG serve as key mediators in coordinating organelle morphology and function (45). DAG activates PKC by binding to the C1 domain, triggering PKC translocation from the cytoplasm to the plasma membrane (46). Moreover, PPARα, a master regulator of lipid metabolism, keeps DAG homeostasis

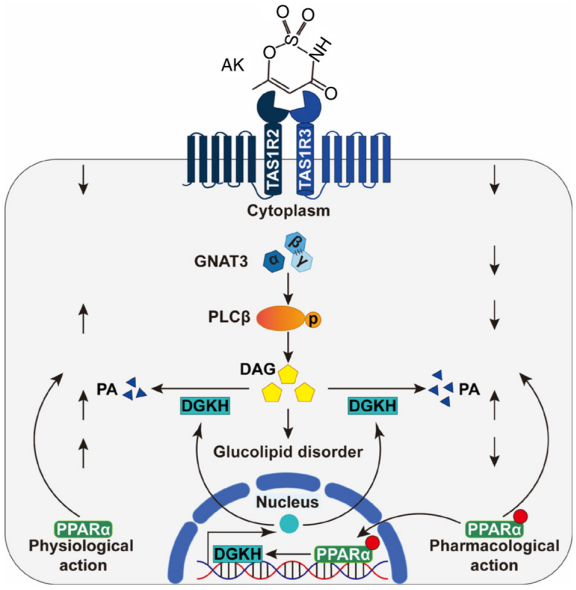

Figure 8. Proposed schematic mechanism by which AK promotes the development of NAFLD dependent on PPARα. The physiological actions of PPARα involve adaptive regulation of STRs, activation of PLCβ, and transcription of DGKH, which mediates DAG catabolism. Pharmacological actions of PPARα downregulate STR signaling via modulation of GNAT3 and PLCβ expression. AK, acesulfame-K; NAFLD, nonalcoholic fatty liver disease; PPARα, peroxisome proliferator-activated receptor α; STR, sweet taste receptor; PLCβ, phospholipase C beta; DGKH, diacylglycerol kinase eta; DAG, diacylglycerol; GNAT3, G protein subunit alpha transducin 3; TAS1R, taste 1 receptor member; PA, phosphatidic acid.

through the transcriptional regulation of lipid-metabolizing enzymes (47,48). In the present study, pharmacologically activated PPARα upregulated both *Dgkh* mRNA expression and DGKH protein expression levels in the WT mice. The lower hepatic DAG levels in the WT mice compared with those in the KO mice likely stemmed from the DGKH regulation by PPARα. Considering the therapeutic role of PPARα agonists in NAFLD treatment, DGKH upregulation by PPARα was hypothesized as a pharmacological pathway balancing hepatic glucolipid metabolism. However, the molecular mechanisms underlying PPARα-DGKH regulation remain to be investigated.

PKCβ acts as a terminal effector of the STR signaling pathway, driving hepatic metabolic reprogramming through lipid partitioning and modulation of glycogen synthesis. Dysregulated PKC signaling in the liver is associated with insulin resistance, impaired glycogen synthesis, and pathological lipid accumulation (49,50). In the present study, pharmacological activation of PPARα markedly downregulated PLCβ and GNAT3 expression levels. The GNAT3/PLCβ/PKC signaling axis emerged as a putative mechanistic pathway through which PPARα activation alleviated NAFLD. While the limited sample size in the present study is acknowledged, the exceptionally large effect sizes observed for primary outcomes lend support to its conclusions. Since the transcription of TAS1R2, TAS1R3, PLCβ, and GNAT3 was not modified by activated PPARα, the mechanisms of the aforementioned regulations remain to be investigated.

Conclusively, chronic AK intake reprograms the hepatic lipid and glucose homeostasis by activating STR signaling. Physiologically, PPARα mediates AK-induced NAFLD by activating the STR signaling component PLCβ. Pharmacologically, activated PPARα suppresses STR signaling via multiple targets, especially PLCβ (Fig. 8). Therefore, dual actions of PPARα in AK induced NAFLD risk may occur via bidirectional regulation of the hepatic PLCβ.

Acknowledgements

The authors thank Dr Chao Dong, technician at the Laboratory Animal Center of Ningbo University, for his technical assistance with animal handling and experimental procedures.

Funding

The present study was supported by the Natural Science Foundation of China (grant nos. 82270602 and 82300654), Natural Science Foundation of Ningbo Municipality (grant nos. 2024J387, 2023J072, 2024J038 and 2022J205), Zhejiang Public Welfare Technology Research Program (grant nos. Y24H030001 and LTGD23H030002), International Sci-tech Cooperation Project (grant no. 2024H001) and the K.C. Wong Magna Fund in Ningbo University.

Availability of data and materials

The data generated in the present study may be requested from the corresponding author. Data generated in the present study may be found in the NCBI BioProject database under accession number PRJNA1397340 or at the following URL: http://www.ncbi.nlm.nih.gov/bioproject/1397340.

Authors' contributions

PYL performed the animal experiments, liver histology, data analysis and drafted the manuscript. JRX conducted biochemical data validation, performed statistical analysis and contributed to funding acquisition. TCQ was responsible for data management. SSW maintained the animal models, monitored metabolic parameters and collected tissue samples. SYY contributed to data analysis and funding acquisition. WBS performed serum biochemical analyses. YW assisted with data visualization, literature review and manuscript formatting. LZC contributed to experimental protocol optimization and provided technical support. QJZ performed histopathological imaging and liver steatosis scoring. YYZ conducted *in vitro* hepatocyte culture and preliminary experiments. HG assisted with sample management and funding acquisition. RF provided technical support for lentiviral transfection experiments. ZXX performed pathological analysis. AML and LX conceived and designed the study, supervised data analysis and quality control, revised the manuscript and contributed to funding acquisition. PYL, AML and LX confirmed the authenticity of all the raw data. All authors read and approved the final manuscript.

Ethics approval and consent to participate

The animal procedures were approved by the Animal Ethics and Welfare Committee of Ningbo University (approval no. AEWC-NBU20230140; Ningbo, China).

Patient consent for publication

Not applicable.

Competing interests

The authors declare that they have no competing interests.

References

1. Feng G, Valenti L, Wong VWS, Fouad YM, Yilmaz Y, Kim W, Sebastiani G, Younossi ZM, Hernandez-Gea V and Zheng MH: Recompensation in cirrhosis: Unravelling the evolving natural history of nonalcoholic fatty liver disease. Nat Rev Gastroenterol Hepatol 21: 46-56, 2024.
2. Loomba R, Friedman SL and Shulman GI: Mechanisms and disease consequences of nonalcoholic fatty liver disease. Cell 184: 2537-2564, 2021.
3. Miao L, Targher G, Byrne CD, Cao YY and Zheng MH: Current status and future trends of the global burden of MASLD. Trends Endocrinol Metab 35: 697-707, 2024.
4. Zhao L, Zhang X, Coday M, Garcia DO, Li X, Mossavar-Rahmani Y, Naughton MJ, Lopez-Pentecost M, Saquib N, Shadyab AH, *et al*: Sugar-sweetened and artificially sweetened beverages and risk of liver cancer and chronic liver disease mortality. JAMA 330: 537-546, 2023.
5. Yki-Järvinen H, Luukkonen PK, Hodson L and Moore JB: Dietary carbohydrates and fats in nonalcoholic fatty liver disease. Nat Rev Gastroenterol Hepatol 18: 770-786, 2021.
6. Jung S, Bae H, Song WS and Jang C: Dietary fructose and fructose-induced pathologies. Annu Rev Nutr 42: 45-66, 2022.

7. Ruiz-Ojeda FJ, Plaza-Díaz J, Sáez-Lara MJ and Gil A: Effects of sweeteners on the gut microbiota: A review of experimental studies and clinical trials. Adv Nutr 10 (Suppl 1): S31-S48, 2019.
8. Magnuson BA, Carakostas MC, Moore NH, Poulos SP and Renwick AG: Biological fate of low-calorie sweeteners. Nutr Rev 74: 670-689, 2016.
9. U.S. Food & Drug Administration (FDA): Aspartame and other sweeteners in food. FDA, Silver Spring, MD, 2024.
10. Spherical Insights: Global Food Sweetener Market Insights Forecasts to 2033. Spherical Insights LLP., Mason, OH, 2025. https://www.sphericalinsights.com/reports/food-sweetener-market.
11. Suez J, Cohen Y, Valdés-Mas R, Mor U, Dori-Bachash M, Federici S, Zmora N, Leshem A, Heinemann M, Linevsky R, *et al*: Personalized microbiome-driven effects of non-nutritive sweeteners on human glucose tolerance. Cell 185: 3307-3328.e19, 2022.
12. Chowdhury CR and Havlik J: Beyond sweetness: A review of the health and safety of acesulfame-K. Food Chem 499: 147290, 2026.
13. Witkowski M, Nemet I, Alamri H, Wilcox J, Gupta N, Nimer N, Haghikia A, Li XS, Wu Y, Saha PP, *et al*: The artificial sweetener erythritol and cardiovascular event risk. Nat Med 29: 710-718, 2023.
14. Wu W, Sui W, Chen S, Guo Z, Jing X, Wang X, Wang Q, Yu X, Xiong W, Ji J, *et al*: Sweetener aspartame aggravates atherosclerosis through insulin-triggered inflammation. Cell Metab 37: 1075-1088.e7, 2025.
15. Zani F, Blagih J, Gruber T, Buck MD, Jones N, Hennequart M, Newell CL, Pilley SE, Soro-Barrio P, Kelly G, *et al*: The dietary sweetener sucralose is a negative modulator of T cell-mediated responses. Nature 615: 705-711, 2023.
16. Ahmad R and Dalziel JE: G protein-coupled receptors in taste physiology and pharmacology. Front Pharmacol 11: 587664, 2020.
17. Nelson G, Hoon MA, Chandrashekar J, Zhang Y, Ryba NJ and Zuker CS: Mammalian sweet taste receptors. Cell 106: 381-390, 2001.
18. Behrens M: Pharmacology of TAS1R2/TAS1R3 receptors and sweet taste. The Pharmacology of Taste. Handbook of Experimental Pharmacology, pp155-175, 2022.
19. Neiers F, Canivenc-Lavier MC and Briand L: What does diabetes 'taste' like? Curr Diab Rep 16: 49, 2016.
20. Ercin M, Gezginci-Oktayoglu S and Bolkent S: Exendin-4 inhibits small intestinal glucose sensing and absorption through repression of T1R2/T1R3 sweet taste receptor signalling in streptozotocin diabetic mice. Transl Res 246: 87-101, 2022.
21. Ubeysinghe S, Wijayaratna D, Kankanamge D and Karunarathne A: Molecular regulation of PLCβ signaling. Integrated Methods in Protein Biochemistry: Part C. Methods in Enzymology, pp17-52, 2023.
22. Pawlak M, Lefebvre P and Staels B: Molecular mechanism of PPARα action and its impact on lipid metabolism, inflammation and fibrosis in non-alcoholic fatty liver disease. J Hepatol 62: 720-733, 2015.
23. Gross B, Pawlak M, Lefebvre P and Staels B: PPARs in obesity-induced T2DM, dyslipidaemia and NAFLD. Nat Rev Endocrinol 13: 36-49, 2017.
24. Chang E, Zhu Y, Wei W, Huai J, Lv T, Lou Y and Zhou X: Chiglitazar, a PPAR pan-agonist: Impacts on type 2 diabetes mellitus and multi-system metabolic regulation-a review. Biomed Pharmacother 193: 118850, 2025.
25. Palacios Girón KM, Hernandez Nazara ZH, Maldonado-González M, Martínez-López E, Sánchez Muñoz MP, Bautista López CA, Aguiñaga MSA, Dominguez-Rosales JA, Vargas-Guerrero B and Ruíz-Madrigal B: Role of ChREBP-PPARα-FGF21 axis in metabolic dysfunction of MASLD. Int J Mol Sci 26: 11425, 2025.
26. Sheetz MJ and King GL: Molecular understanding of hyperglycemia's adverse effects for diabetic complications. JAMA 288: 2579-2588, 2002.
27. Reagan-Shaw S, Nihal M and Ahmad N: Dose translation from animal to human studies revisited. FASEB J 22: 659-661, 2008.
28. Hua H, Dai M, Luo Y, Lin H, Xu G, Hu X, Xu L, Zhang H, Tang Z, Chang L, *et al*: Basal PPARα inhibits bile acid metabolism adaptation in chronic cholestatic model induced by α-naphthylisothiocyanate. Toxicol Lett 300: 31-39, 2019.
29. Luo J, Yan Z, Dai M, Xu L, Zhang H, Xi Y, Yang J and Liu A: Down-regulation of hepatic CLOCK by PPARα is involved in inhibition of NAFLD. J Mol Med (Berl) 101: 139-149, 2023.
30. Wang X, Luo J, Lu Z, Fang S, Sun M, Luo W, Shen J, Liu A and Ye H: Therapeutic effect of fenofibrate for non-alcoholic steatohepatitis in mouse models is dependent on regime design. Front Pharmacol 14: 1190458, 2023.
31. Kojima I and Nakagawa Y: The role of the sweet taste receptor in enteroendocrine cells and pancreatic β-cells. Diabetes Metab J 35: 451-457, 2011.
32. Livak KJ and Schmittgen TD: Analysis of relative gene expression data using real-time quantitative PCR and the 2(-Delta Delta C(T)) method. Methods 25: 402-408, 2001.
33. Laviada-Molina H, Molina-Segui F, Pérez-Gaxiola G, Cuello-García C, Arjona-Villicaña R, Espinosa-Marrón A and Martinez-Portilla RJ: Effects of nonnutritive sweeteners on body weight and BMI in diverse clinical contexts: Systematic review and meta-analysis. Obes Rev 21: e13020, 2020.
34. Allende DS, Gawrieh S, Cummings OW, Belt P, Wilson L, Van Natta M, Behling CA, Carpenter D, Gill RM, Kleiner DE, *et al*: Glycogenosis is common in nonalcoholic fatty liver disease and is independently associated with ballooning, but lower steatosis and lower fibrosis. Liver Int 41: 996-1011, 2021.
35. Hindmarsh JT, Kilby D and Wiseman G: Effect of amino acids on sugar absorption. J Physiol 186: 166-174, 1966.
36. Mace OJ, Affleck J, Patel N and Kellett GL: Sweet taste receptors in rat small intestine stimulate glucose absorption through apical GLUT2. J Physiol 582: 379-392, 2007.
37. Korenfeld N, Charni-Natan M, Bruse J, Goldberg D, Marciano-Anaki D, Rotaro D, Gorbonos T, Radushkevitz-Frishman T, Polizzi A, Nasereddin A, *et al*: Repeated fasting events sensitize enhancers, transcription factor activity and gene expression to support augmented ketogenesis. Nucleic Acids Res 53: gkae1161, 2025.
38. Kim H, Zheng Z, Walker PD, Kapatos G and Zhang K: CREBH maintains circadian glucose homeostasis by regulating hepatic glycogenolysis and gluconeogenesis. Mol Cell Biol 37: e00048-17, 2017.
39. Kersten S, Seydoux J, Peters JM, Gonzalez FJ, Desvergne B and Wahli W: Peroxisome proliferator-activated receptor alpha mediates the adaptive response to fasting. J Clin Invest 103: 1489-1498, 1999.
40. Lee B, Ghumman U, Pedicone LD, Aldana AG and Lawitz E: Prospects of late-stage development agents in the treatment of metabolic dysfunction-associated steatohepatitis. Clin Mol Hepatol 31: 1167-1196, 2025.
41. Tan Y and Pang X: Olfactory-gustatory cross-modal integration: Mechanisms of aroma-induced sweetness enhancement, sensory evaluation methodologies, neuroimaging evidence and advances in influencing factors. J Adv Res: S2090-1232(25)00745-3, 2025 (Epub ahead of print).
42. Kawano T, Inokuchi J, Eto M, Murata M and Kang JH: Activators and inhibitors of protein kinase C (PKC): Their applications in clinical trials. Pharmaceutics 13: 1748, 2021.
43. Domingues N, Pires J, Milosevic I and Raimundo N: Role of lipids in interorganelle communication. Trends Cell Biol 35: 46-58, 2025.
44. Sarmento MJ, Llorente A, Petan T, Khnykin D, Popa I, Nikolac Perkovic M, Konjevod M and Jaganjac M: The expanding organelle lipidomes: Current knowledge and challenges. Cell Mol Life Sci 80: 237, 2023.
45. Ulch BA, Clews AC, Reisiger CA, Zhu LH, Mullen RT, Kimber MS and Xu Y: Properties and biochemistry of phosphatidylcholine: Diacylglycerol cholinephosphotransferase. Prog Lipid Res 101: 101361, 2025 (Epub ahead of print).
46. Katan M and Cockcroft S: Phospholipase C families: Common themes and versatility in physiology and pathology. Prog Lipid Res 80: 101065, 2020.
47. Finck BN, Lehman JJ, Leone TC, Welch MJ, Bennett MJ, Kovacs A, Han X, Gross RW, Kozak R, Lopaschuk GD and Kelly DP: The cardiac phenotype induced by PPARalpha overexpression mimics that caused by diabetes mellitus. J Clin Invest 109: 121-130, 2002.
48. Montaigne D, Butruille L and Staels B: PPAR control of metabolism and cardiovascular functions. Nat Rev Cardiol 18: 809-823, 2021.
49. Shu Y, Hassan F, Ostrowski MC and Mehta KD: Role of hepatic PKCβ in nutritional regulation of hepatic glycogen synthesis. JCI Insight 6: e149023, 2021.
50. Zheng ZG, Xu YY, Liu WP, Zhang Y, Zhang C, Liu HL, Zhang XY, Liu RZ, Zhang YP, Shi MY, *et al*: Discovery of a potent allosteric activator of DGKQ that ameliorates obesity-induced insulin resistance via the sn-1,2-DAG-PKCε signaling axis. Cell Metab 35: 101-117.e11, 2023.

Copyright © 2026 Lin et al. This work is licensed under a Creative Commons Attribution-NonCommercial-NoDerivatives 4.0 International (CC BY-NC-ND 4.0) License.